Radon Activity in Volcanic Gases of Mt. Etna by Passive Dosimetry

Luca Terray, Pierre-Jean Gauthier, Vincent Breton, Salvatore Giammanco, Olgeir Sigmarsson, Giuseppe Salerno, Tommaso Caltabiano, Alain Falvard

Radon activity in volcanic gases of Mt. Etna by passive dosimetry

Luca Terray[1,2], Pierre-Jean Gauthier[1], Vincent Breton[2], Salvatore Giammanco[3], Olgeir Sigmarsson[1], Giuseppe Salerno[3], Tommaso Caltabiano[3] and Alain Falvard[2].

[1] Laboratoire Magmas et Volcans, Université Clermont Auvergne, Aubière, France

[2] Laboratoire de Physique de Clermont, Université Clermont Auvergne, Aubière, France

[3] Istituto Nazionale di Geofisica e Vulcanologia, Osservatorio Etneo, Catania, Italy

Abstract

Radon (^{222}Rn) activity in air was measured for about six months at the summit of Mt. Etna Central Crater (Sicily) by integrative radon dosimetry at two different heights above ground level (5 cm and 1 m). This technique for air radon monitoring proved operational in the harsh volcanic environment of Mt. Etna summit with a 94% recovery rate of dosimeters. In the South-East sector exposed to the main gas plume, mean radon activity in free air (height 1 m) is significantly higher than the local background and the ground level activity (height 5 cm). The results strongly suggest that the plume is enriched in radon by ≈ 550 Bq/m^3, which has never been evidenced before. Radon activities also reflect soil degassing occurring in the proximity of the crater, with increased ground level activities in zones of enhanced soil fracturing and degassing. Radon measurements also revealed a hotspot in front of the Voragine vent with extraordinary high levels of air activities (26 kBq/m^3 at ground level and 8 kBq/m^3 in free air). The temporal variation of radon activity was investigated by replacing a few stations half way through the exposure period. The only significant increase was associated with the site located under the main gas plume and correlated with eruptive unrest within the crater. Finally, air radon levels higher than the recommended threshold of 300 Bq/m^3 were detected in several zones on the rim and could generate a non-negligible radiologic dose for workers on the volcano.

1) Introduction

[1] Radon (^{222}Rn) is a radioactive noble gas produced by the decay of ^{226}Ra. As such, radon abundance is generally high in U-bearing geological formations, including volcanic and geothermal zones (e.g., Monnin, 2001). Since the pioneering work of Chirkov at Karymsky volcano, Kamchatka (Chirkov, 1975), radon measurements at active volcanoes, either in fumaroles or in soil gases, have been carried out worldwide in order to investigate radon activity variations as a precursory monitoring tool (see recent reviews by Cigolini et al., 2016 and Morales-Simfors et al., 2020, and references therein). Albeit promising, the radon signature in soil gases and/or fumarolic discharges appears however not always easy to decipher. Besides the well-known diurnal and seasonal variation of radon emissions related to meteorological effects and earth tides, radon activities can indeed be affected by local variations of soil temperature and humidity, local stress regime constraints and other parameters which may hide the signature of magmatic processes at depth (Zimmer and Erzinger, 2003; Cigolini et al., 2016; Mollo et al., 2018).

[2] The primary magmatic vapor released in gaseous plumes at open-conduit degassing volcanoes thus could be an ideal candidate to investigate radon anomalies directly linked to magmatic processes at depth. Unfortunately, almost no systematic survey of in-air radon activities in volcanic plumes have been carried out so far, apart from a single study on short-lived ^{222}Rn daughters at Mount Erebus, Antarctica (Polian and Lambert, 1979). In marked contrast, emissions of the last three radon daughters (namely ^{210}Pb, ^{210}Bi and ^{210}Po) in volcanic plumes have been well established for more than 40 years (e.g., Lambert et al., 1976). The study of ^{210}Pb-^{210}Bi-^{210}Po radioactive disequilibria in magmatic gases

58 has proved efficient to infer degassing dynamics of active volcanic systems, either in a state of open-
59 conduit persistent degassing (Lambert et al., 1985; Gauthier et al., 2000; Le Cloarec and Pennisi, 2001;
60 Allard et al., 2016), in an eruptive dome setting (Le Cloarec and Gauthier, 2003) or during lateral fissure
61 eruptions (Gauthier et al., 2016).

62 **[3]** Early experiments by Sato et al. (1980) suggested that radon is thoroughly degassed from liquid
63 silicates at magmatic temperatures, a finding later confirmed by radon analyses of freshly erupted
64 lavas (Gill et al., 1985). However, an experimental investigation of radon diffusion in andesitic melts
65 (Gauthier et al., 1999) suggested that complete radon degassing is achieved only when major gas
66 species (mostly CO_2 and H_2O) act as a radon carrier. Indirect evidence of sustained radon degassing
67 from erupting magmas can be found in the observation of large ^{210}Pb deficits over ^{226}Ra in some recent
68 lavas (e.g., Gauthier and Condomines, 1999; Berlo et al., 2006). Meanwhile, ^{210}Pb excesses over ^{226}Ra
69 have been observed elsewhere suggesting the reverse behavior, that is radon accumulation at depth
70 followed by its subsequent radioactive decay within the magma (e.g., Berlo et al., 2006; Condomines
71 et al., 2010; Sigmarsson et al., 2015). The question whether radon is efficiently released through
72 outgassing of magmatic volatiles at volcanic craters or decays out at depth, due to its relatively short
73 half-life of 3.8 days, remains largely unanswered because magmatic plume emissions of radon have
74 not yet been documented.

75 **[4]** In May 2018, we installed a network of radon passive dosimeters all around the rim of Mt. Etna
76 Central Crater, in Sicily. The dosimeters were left on site for about five months (from May 24, 2018 to
77 October 11, 2018), until their retrieval for the laboratory determination of radon activity. The first goal

of the study was to determine mean radon levels in the air around the crater in order to constrain radon emissions related to volcanic plume, fumaroles, high soil degassing, or a combination of these various sources. The second goal of the study was to test the capability of radon measurements in air to be part of the monitoring system of active volcanoes, Mt. Etna being one of the best monitored volcano laboratory in the world (Bonaccorso et al., 2004). Finally, this study was also aimed at assessing the potential radiologic hazard associated to high radon levels in air around the crater, since Mt. Etna summit is systematically visited every year by thousands of tourists, scientists and volcanological guides, and health hazards related to volcanic gas plumes are often pointed out (Delmelle et al., 2002; Hansell and Oppenheimer, 2004).

2) Area of study

[5] Mt. Etna is a stratovolcano located on the east coast of Sicily and one of the most active volcanoes in Europe. Its edifice is a 3300 m above sea level (a.s.l.) high cone with a collapsed eastern flank (Valle del Bove) and a complex summit morphology (e.g., Neri et al., 2017) composed of three different groups of active craters (see Figures 1 and 2): (i) the Central Crater (CC) hosting two inner craters named Bocca Nuova (BN) and Voragine (VOR), (ii) the North-East Crater (NEC), and (iii) the South-East Craters. Its present eruptive activity is characterized by diverse eruptive styles, from purely effusive to mild and violent strombolian with very energetic lava fountains (e.g., Allard et al., 2016). In addition, Mt. Etna is often classified as an open-conduit volcano because of the continuous emission of large quantities of magmatic gases from its main craters (Aiuppa et al., 2008; Salerno et al., 2009a). An active hydrothermal system is also located at shallow depth beneath its summit (Liotta et al., 2010).

98 **[6]** This study focused on the Central Crater because persistent passive or active plume emissions from
99 Bocca Nuova and Voragine vents ensured an almost continuous presence of magmatic gases on the
100 crater rim, whereas other craters were mostly emitting gas through fumarole fields. The degassing
101 regime of the Central Crater between May and October 2018 reflects the recent eruptive activity:

102 - (i) BN and VOR craters merged after the December 2015 and May 2016 paroxysmal eruptions and
103 eruptive products totally filled the two craters (Corsaro et al., 2017; Marchese et al., 2018).
104 Subsequently, the tectonic structure of the summit was considerably modified and a swarm of North-
105 South oriented fractures opened from the North-East Crater to the South-East Craters, passing east of
106 the Central Crater (Fig. 1a; see also Marchese et al., 2018). It led to both enhanced fumarolic activity
107 and increased diffuse soil degassing within the Central Crater and around it (see for instance Figure 3
108 in Marchese et al., 2018). Our field observations suggest that this degassing activity was still present,
109 albeit at lower intensity, in 2018 at the time of the study.

110 - (ii) Since May 2016, BN and VOR craters have been subsiding, progressively reforming the former
111 geometry of the Central Crater. In August 2016, a degassing pit opened on the inner east flank of VOR
112 crater twenty meters below the rim (Marchese et al., 2018; VOR vent, see Figures 1 and 2), apparently
113 draining most of diffuse emissions nearby and remained active in 2018 at the time of our
114 measurements. In early 2018, a new degassing pit opened on the west side of BN crater floor (BN1,
115 see Figures 1 and 2), where most of the degassing activity took place.

116 - (iii) In late May/early June 2018, at the start of the experiment, activity mostly consisted in sustained
117 degassing from the BN1 vent, and additional mild degassing at the NE Crater (Figure 2). In the course

of summer 2018, a slight unrest occurred in the eruptive activity as witnessed by thermal anomalies observed from the Sentinel imager satellite (Figure 2) and other remote sensing approaches (Marchese et al., 2019), as well as an increase in SO_2 fluxes (see Supplementary Material) and volcanic tremor (e.g., *Bollettino settimanale sul monitoraggio vulcanico, geochimico e sismico del vulcano Etna, 20/08/2018 - 26/08/2018*, 2018). Magmatic explosions were further reported by witnesses at BN (explosion bangs and visual observations of volcanic bombs ejected from the craters), this unrest period culminating in the opening of a new vent on the east side of the BN crater (BN2, see Figures 1 and 2) in August 2018 (see Figure 4 in Marchese et al., 2019).

[7] Beside the activity at Central Crater, major eruptive events during the 2016-2018 period included a sequence of six effusive eruptions at South East Craters in February-March 2017 (De Beni et al., 2019), a short strombolian and effusive episode at New South East Crater by late August 2018 and a lateral fissure eruption in December 2018 (De Novellis et al., 2019).

3) Methods

[8] A temporary network of radon passive dosimeters was deployed for five months (from May to October 2018) around the Central Crater of Etna and in the close vicinity of the summit area in order to assess radon levels at Mt. Etna summit. The network initially consisted in 29 monitoring stations set on the Central Crater rim (yellow and purple dots in Figure 1a) and 3 reference stations at distance from the summit area (La Montagnola, Pizzi Deneri, Torre del Filosofo, Fig. 1b). An example of radon station is shown in Figure 3. It consists of two dosimeters (one at ground level - i.e., 5 cm above ground - and one in free air - i.e., at 1 m elevation) fixed to a 1.5 m high wooden stick solidly anchored to the

ground. This configuration was chosen in order to discriminate the contribution of soil radon emissions from that of plume radon emissions. The bottom dosimeter would indeed mostly reveal the intensity of very local soil emissions while the top dosimeter will also be sensitive to radon from further distant sources and transported by the wind (such as degassing vents). In July 2018, dosimeters at five monitoring stations were picked up for analysis and immediately replaced by new dosimeters. Additionally, a fourth reference station was installed further from the summit area, down in the Valle del Bove (Fig 1b). As a whole, no less than 76 passive dosimeters were used for this experiment.

[9] For this experiment, we used DPR2 dosimeters provided by the Algade company (Bessines-sur-Gartempe, France). These dosimeters are made of a LR-115 (cellulose nitrate) sensitive film, encapsulated in a sealed plastic half-dome in order to prevent both thoron (^{220}Rn) and radioactive aerosol particles from contributing to the measurement. The Algade company indicates a minimum exposure period of two months (indoor conditions) in order to properly measure a radon activity of about 20 Bq/m^3. Although LR-115 films had been previously used to measure in-soil radon activities on volcanoes (e.g., Seidel and Monnin, 1984), they were used for the first time in outdoor conditions on a volcano during the present study. It was thus decided to leave dosimeters in the field for the whole summer period (May 24 – October 11) in order to ensure sufficient radon exposure. Nonetheless, five crater stations were replaced on the 6th of July 2018 with several objectives: (i) validate the methodology by checking that cellulose nitrate films were not corroded by acid gases and damaged by moisture, (ii) check the exposure level after two months in order to avoid film saturation and (iii) look for potential temporal variations between May-July and July-October 2018. After collection of the passive dosimeters in the field, they were sent to the Algade laboratory (within two days) where the

159 films were analyzed (see previous studies using LR-115 films for further methodological and analytical
160 details; e.g., Seidel and Monnin, 1984). Radon activities were obtained within two weeks, with a global
161 2σ uncertainty (counting statistics, calibration error, error due to temperature variations during the
162 chemical processing of the dosimeter, error coming from the slightly variable quality of the sensitive
163 films).

164 **[10]** Because passive dosimetry integrates radon activity in air over a long period of time (weeks to
165 months), it filters out the large variability of radon activity in air due to short-period (< 1 day)
166 fluctuations, often inherited from meteorological fluctuations (e.g. Zimmer and Erzinger, 2003). As
167 such, it is an easy-to-deploy and low-cost technics allowing determination of a mean value
168 representative of radon emission and accumulation at a given place over a given time period.
169 Moreover, a dosimeter does neither require a power supply nor data logging system and it can be
170 installed for several months even in harsh outdoor conditions without damage.

171 **[11]** In order to identify the zone under volcanic plume influence, wind direction and intensity over
172 the crater during the experiment period, May to October 2018, are needed. We used open-access data
173 acquired by radiosondes launched twice a day at Trapani in western Sicily
174 (http://weather.uwyo.edu/upperair/sounding.html). Wind direction and horizontal wind speed were
175 obtained from each radiosonde profile, selecting the values measured in the range of elevation of Mt.
176 Etna summit craters (between 3000 and 3400 meters a.s.l.). Although radiosonde data refer to a site
177 located 220 km away from Mt. Etna, high-altitude winds are relatively stable over long distances,
178 especially when there is no obstacle from the terrain in between, as it is the case of Sicily where no

3000m-high mountains exist apart from Mt. Etna. Trapani data are thus a good proxy for Mt. Etna high-altitude wind-field, as evidenced in other studies on Mt. Etna's plume (e.g., Scollo et al., 2014).

4) Results

[12] Out of 76 installed dosimeters, only three were missing at the end of the experiment. All films but one could be analyzed and did not present any sign of acid degradation. A single pair of dosimeters was clogged into a cm-thick crust of soldered dust and therefore excluded from the dataset as it was impossible to determine if radon could still enter the capsule. We finally obtained a global recovery rate of 94% (number of interpretable dosimeters/number of installed dosimeters). This demonstrates that passive dosimetry is a technique suitable for harsh outdoor volcanic conditions (windy, cold, humid and acid atmosphere).

4.1 Spatial distribution of radon anomalies

[13] All results and station details are given in Table 1. The overall uncertainty on obtained ^{222}Rn activities varies between 14% and 38% with a mean value of 22% (2σ relative uncertainty). Reference stations located far from the active crater zone (see Figure 1b) present a mean activity of 63 ± 18 Bq/m^3 at ground level and a mean activity of 36 ± 9 Bq/m^3 at a meter above the ground (free air). Higher values near the ground are not surprising because the only source of radon far from degassing vents is soil degassing. The activity found in free air is in qualitative agreement with previous radon measurements in the outdoor air of Mt. Etna region, ranging from 3 to 20 Bq/m^3 (Vaupotič et al., 2010).

[14] Radon activities measured on the crater rim are characterized by a high variability: ground level activities are found in the range 40 - 26,000 Bq/m^3, while free air activities range from 37 to 8800

199 Bq/m^3. Despite these wide ranges of values, geographical patterns can be observed. Figures 4a and 4b
200 represent the spatial distribution of integrated ground-level and free-air radon activities measured at
201 each station in the main four sectors of the crater rim (North-West, North-East, South-East and South-
202 West), as well as the wind directions during the exposure period. The main wind direction is from NW
203 to SE with an occurrence percentage > 80%. It is noteworthy that the NW sector presents the lowest
204 ground-level and free-air activities among those recorded all around the crater. In this sector, mean
205 activity at ground level (82 ± 17 Bq/m^3) is in agreement with the respective mean background activity
206 measured at reference stations (63 ± 18 Bq/m^3) while mean activity in free air (71 ± 13 Bq/m^3) is slightly
207 higher than reference stations mean value (36 ± 9 Bq/m^3). No statistical difference between the two
208 elevations is found, even though the mean ground-level activity is slightly higher than the mean free-
209 air activity. Both NE and SW sectors show a very similar pattern with significantly higher ground-level
210 activities (155 ± 43 and 186 ± 62 Bq/m^3, respectively) but low free-air activities (75 ± 10 and 90 ± 15
211 Bq/m^3, respectively) similar to those in the NW sector. Finally, the SE sector presents the highest mean
212 values of both ground-level and free-air activity with mean free-air activity (704 ± 409 Bq/m^3) markedly
213 higher than mean ground-level activity (301 ± 114 Bq/m^3). This latter pattern implies the contribution
214 of an external radon source (i.e., different from soil degassing) transported by the wind. Since the two
215 main degassing vents of Bocca Nuova (BN1 and BN2) and the SE sector of the crater rim are aligned
216 along the main wind direction, these results strongly suggest that the observed radon anomaly might
217 be associated with the gas plume released by BN. This observation is the first direct evidence that
218 magmatic gases released in the main crater plume of Mt. Etna are significantly enriched in radon.

[15] Ground-level radon anomalies observed both in the SW and NE sectors of the crater rim are coherent with the degassing phenomenology observed in the field. The SW sector of Mt. Etna's Central Crater mostly consists of a terrace covered by a massively altered yellow soil that likely results from the chemical alteration of basaltic rocks by acidic soil gases. The NE sector is a highly fractured zone (Marchese et al., 2018; see also Figure 1a) that also presents many features of severe soil alteration. Both sectors are sites of elevated soil CO_2 diffuse degassing (Giammanco et al., 2016) that is likely associated with important radon soil emanations that can produce a significant radon anomaly at ground level. They are also areas of intense fumarolic activity as witnessed by the water vapor intensity seen in Sentinel images (see Figure 2). In marked contrast, important diffuse or fumarole degassing was not observed in the NW sector, which is in agreement with the low levels of radon activity measured close to ambient background.

[16] A hotspot of anomalous radon emission was also identified near the Voragine degassing vent (at the station located twenty meters upslope of the vent, see Figure 1a). At ground level, radon activity reaches 26,000 Bq/m^3 whereas at 1 m height, it is 8,800 Bq/m^3. No equivalent activity levels were found elsewhere around the crater including at stations adjacent to the hotspot site, and no progressive increase of radon activity towards it can be observed. It suggests that the hotspot is due to a very localized and peculiar structure, likely related to the strong degassing from the Voragine vent. In any case, this station was excluded from the computation of the sector mean radon activity.

4.2 Temporal evolution of radon anomalies

238 **[17]** Figure 5 represents, for each of the four sectors around the Central Crater (Fig. 5a to 5d), the
239 temporal evolution of radon activity at stations that were retrieved and immediately replaced in July
240 2018. Coherent patterns between the two periods of exposure can be observed for the different
241 sectors, although only one pair of dosimeters (ground-level and free-air) has been collected and
242 analyzed from each sector. For the two northern sector stations (NW and NE), free-air integrated radon
243 activities decreased (NW) or increased (NE) by a factor of ~2 during the second period of exposure but
244 remained within the range of reference values, in agreement with the hypothesis of limited influence
245 of the gas plume. Ground-level activities increased by a factor of ~3 in both cases and exhibit values
246 significantly higher than the reference level (Fig. 5a and 5b). This pattern could be tentatively
247 interpreted as resulting from enhanced soil degassing during the second period although a
248 meteorological effect , for instance due to an increased stability of the surface air layer, cannot be
249 ruled out. The two southern sector stations (SW and SE) are both characterized by a decrease in radon
250 activity at ground-level between the two periods (by a factor or ~2), hence producing values at the
251 reference level (Fig. 5c and 5d). In marked contrast, free-air radon activities are significantly higher and
252 above the reference value, which is especially obvious for the SE station where radon activity at 1 m
253 above ground level is 15 times higher than during the first period of exposure. Such decoupling
254 between ground-level and free-air activities excludes any interpretation based on a modification of
255 the local soil radon flux (either from meteorological or volcanological origin). In which case, an even
256 more important increase of ground-level activity should have been observed too. In fumaroles,
257 rainfalls can trigger positive radon anomalies but such induced radon enrichments usually are of much
258 lower magnitude (Zimmer and Erzinger, 2003). Furthermore, weather conditions during the whole

period of the experiment were rather calm, with rare rainy events evenly distributed at the end of the spring season and the beginning of the fall season. Since both wind direction and speed were similar during May-Jul and Jul-Oct periods (see Fig. 5e and 5f), it can thus be suggested that the tremendous increase in free-air radon activity observed at the SE station is related to the volcanic plume itself, especially because this station was installed in the windiest part of the SE sector (Fig. 4), downwind the active Bocca Nuova vents. Although sustained degassing activity occurred throughout the study period, it is worth noting that several signs of volcanic unrest were noticed, starting mid-July 2018 right after the new sets of dosimeters were installed around the crater rim. Evidences for this unrest may be found in the occurrence of strombolian explosions within the Central Crater (see also section 2 and Marchese et al., 2019), increasing thermal anomalies (Fig. 2), increasing SO_2 fluxes (see Supplementary Material) and higher tremor with noticeable excursions into the red alert zone (e.g., *Bollettino settimanale sul monitoraggio vulcanico, geochimico e sismico del vulcano Etna, 20/08/2018 - 26/08/2018,* 2018). It thus suggests a correlation between stronger magmatic activity at the summit craters and increased radon activity in the air (and possibly also at the ground level) at the summit area of the volcano (see discussion hereafter).

5) Discussion

5.1 Radon enrichments in Mt. Etna gas plume

[18] In each summit sector of the volcano where the plume contribution is low or even virtually negligible (reference stations, NW, NE (including the Voragine hotspot) and SW sectors), the ratio of free-air to ground-level radon activities (termed hereafter air-soil ratio) range from 0.33 ± 0.23 to 0.86

± 0.37, with an average value of 0.53 ± 0.20. In marked contrast, the air-soil ratio in the SE sector averages 2.34 ± 0.85. Together with the high mean free-air activity observed in the same sector, this suggests a significant radon enrichment in the crater plume compared to the atmospheric background, in agreement with a theoretical model that proposed high plume emissions of radon from open-conduit volcanoes due to the persistent regeneration of radon in the degassing reservoir at depth by the decay of non-volatile ^{226}Ra (Terray et al., 2018). In order to quantify this enrichment, the local contribution of soil degassing must be taken into account and subtracted. To do so, we assume that the air-soil ratio of 0.53 ± 20 represents the typical vertical gradient of radon activity in air from soil degassing in the absence of external aerial sources, which is in qualitative agreement with 1D vertical turbulent diffusion models (Jacobi and André, 1963). It can be tentatively assumed that such a vertical gradient also applies to the SE sector of Mt. Etna Central Crater. Therefore, it is possible to compute that the contribution from radon soil emanation at 1 m above ground level is 0.53 × 301 (mean ground level activity) = 160 Bq/m^3. Considering the average free air radon activity for the SE sector (704 Bq/m^3, Table 1), this leads to a radon enrichment in the plume of 704 – 160 ≈ 550 Bq/m^3.

[19] This figure is the first direct estimate of radon activity in a gas plume released by an open-conduit volcano. Nonetheless, a previous study on Mount Erebus (Polian and Lambert, 1979) dealt with plume activities of aerosol-attached ^{218}Po (the first daughter of ^{222}Rn) in the range 170-586 pCi/m^3 (6.3-21.7 Bq/m^3). The comparison of these two estimates is not straightforward since significant radioactive disequilibria prevail between radon and its first daughter in the lower atmosphere ((^{218}Po/^{222}Rn) activity ratio as low as 0.45 during summertime, e.g. Kojima, 1996). Furthermore, a significant fraction of ^{218}Po atoms is not attached to aerosol particles and cannot be sampled by standard filtration

methods (Tokonami et al., 1996), this fraction of unattached atoms being preponderant in water-saturated atmospheres like volcanic plumes. Accordingly, the estimate proposed by Polian and Lambert (1979) must be regarded as a minimum value. Conversely, our estimate of radon activity in the volcanic plume is one order of magnitude lower than that measured in mid-temperature fumarole discharges from VOR Crater (Giammanco et al., 2007). Because many fumaroles are located on the inner walls of the Central Crater and along the fracture swarm extending from North-East Crater to South-East Craters (Figure 1a), it cannot be ruled out that they contributed to the radon activity measured by our monitoring stations. This contribution however, likely remains moderate since active fissures in the SE sector are mostly located downslope the summit flank (Fig. 1a), so that dominant winds blow fumarolic gases away from our monitoring stations. Whatever be this contribution, the value of 550 Bq/m^3 for the bulk volcanic plume in the SE sector thus should be regarded as a maximum estimate, albeit realistic.

5.2 Spatial variability of radon activity and degassing pathways

[20] As previously discussed and apart from the Voragine hotspot, the highest radon activities were measured in the SE sector of the Central Crater, which is the most exposed area to the volcanic plume during the study period. Looking into more details, a significant variability of free-air radon activities is observed in this sector (Table 1). The three southernmost stations in the SE sector show relatively medium to high values (in the range 80-222 Bq/m^3) whereas the two northernmost stations measured up to 2500 Bq/m^3, the highest value recorded in free-air at the summit of Mt. Etna, with the exception of the VOR hotspot. These two latter stations were located not only in the windiest subsector of the

SE sector (Fig. 4b), but also the closest to the BN2 vent, a few tens of meters downwind. Furthermore, passive dosimeters at one of these two stations were retrieved in July 2018 and immediately replaced by new ones. While radon activity at this station remained moderate between May and July (73 ± 20 Bq/m^3), a sharp increase was noticed for the second period, peaking at 1091 Bq/m^3. Interestingly, the BN2 vent opened and started to be active on August 16, 2018, which implies that the gas released from the new vent could be associated with the observed radon increase during the second period of exposure. This could be due either to a lower dilution of the gas plume arising from BN2, or to a higher content of radon in the gas discharge from the new BN2 vent. No matter what scenario applies best, these results suggest that a change in the degassing process – through the opening of a new vent – can be tracked through radon monitoring in air.

[21] The situation is rather different for the Voragine hotspot, where the highest radon activity is found at ground level. At this station, free-air radon activity could merely result from the vertical gradient of radon diffusion from soil to air at 1 meter above ground level (air-soil ratio of 0.33). The high radon activity at this place, thus, does not necessarily implies that the plume issued from VOR vent was particularly enriched in radon. Nevertheless, extremely high radon activities next to the VOR vent are not puzzling, even at ground level. This vent formed in August 2016 in a zone that was highly fractured by the 2015-2016 paroxysmal episodes at Voragine Crater. Before the vent opening, those fractures served as main pathways for soil gas emissions and fumarole discharges while the main degassing vents within the Voragine were still plugged (Marchese et al., 2018)**.** When the radon monitoring station was installed in 2018, we measured a soil temperature of 360°C at a depth of 30 cm with a Type K thermocouple placed within one sealed crack on the eastern rim of Voragine, just nearby the station

341 that recorded the radon hotspot. Therefore we propose that the fissure swarm on the eastern rim of
342 Voragine was one of the most permeable part of the crater structure, allowing deep gas ascent, as
343 suggested for a previous eruptive cycle (Giammanco et al., 2007).

344 *5.3 Temporal variability of radon activities as a tool for volcano monitoring?*

345 **[22]** As shown in Figures 5a to 5d, a marked temporal evolution between the two exposure periods in
346 each sector of the volcano was observed. While ground-level emissions of radon appear slightly higher
347 during the second period on the northern side of Central Craters, free-air activities are markedly
348 enriched on the southern side, especially at that station most exposed to dominant wind in the SE
349 sector (Figure 5). It suggests that most radon emissions, either through soil degassing or by plume
350 outgassing, occurred during the period July-October 2018 when the volcano was more active.
351 Increased radon activities in soils were previously noted during eruptive periods at Mt. Etna, notably
352 on the southern flank of the summit area (Neri et al., 2016). However, this is the first time that an
353 increase in radon activity is observed in a gaseous plume released from the craters of an open-conduit
354 volcano. A simple wind effect due to a change in wind direction can be ruled out since the wind regime
355 remained stable between the two periods (Fig. 5e and 5f). In the meantime, as the summit craters
356 were progressively reactivating, SO_2 flux analysis suggests a gradual increase of the degassing activity
357 between May and October 2018 (see Supplementary Material). Even though the day-to-day variability
358 of SO_2 flux is high, both mean and maximum SO2 fluxes are higher during the second period as well as
359 the detrended cumulated SO_2 flux values (see Supplementary Material). Although the time-evolution
360 of radon activity in the plume of Etna is based on rather limited number of samples, its apparent

361 correlation with SO_2 fluxes in a period of progressive unrest may give expectancies for the potential of
362 in-air radon measurements as a tracer of volcanic activity.

363 **[23]** Furthermore, while radon activity in the volcanic plume could be up to 15 times higher during the
364 July-October period (Table 1; Figure 5), it is worth noting that the SO_2 flux showed a much more limited
365 increase, by about 10% (see Supplementary Material). It is well known that variations in SO_2 fluxes
366 released in the atmosphere are directly proportional to the magma influx at depth (Andres et al., 1993).
367 Hence, despite slightly increased SO_2 degassing during the second period, it can be assumed that the
368 amount of magma degassing per unit of time did not drastically change between the two periods. In
369 such a case, theoretical models predict that the flux of radon produced in the degassing magma is
370 constant (Terray et al., 2018). However, because radon is a radio-isotope with a short half-life (3.8
371 days), radon activity in the gas phase can vary according to the transfer time of gases from the
372 degassing reservoir to the surface (Terray et al., 2018). We can assume that the 15 times increase in
373 radon activity between the two exposure periods was solely due to a transfer time variation, which
374 would be the case if the mean plume dilution rate at the monitoring station was not significantly
375 different for the two periods and if the contribution of steaming fumaroles was negligible. An increase
376 in radon activity by a factor of 15 would be achieved in 3.9 radon half-lives. In other words, the
377 observed increase in radon activity could be explained by a transfer time of gases 15 days shorter after
378 the beginning of the July 2018 volcanic unrest. The ^{210}Pb-^{210}Bi-^{210}Po systematics in Mt. Etna gases
379 allowed estimating a gas transfer time in the range of 1-3 days during eruptive events (Terray et al.,
380 2018) and up to 17 days during quiescent degassing (Lambert et al., 1985). Although the 15-day shorter
381 transfer time deduced from the present study corresponds to a maximum estimate, it is in fair

382 agreement with the difference between the estimates of Lambert et al. (1985) and those of Terray et
383 al. (2018). It thus suggests, in agreement with the moderate increase in SO_2 flux, that the summer 2018
384 eruptive activity was not triggered by an important reinjection of deep volatile-rich magma in the
385 shallow plumbing system but instead by the shallower degassing of the already present magma batch
386 (shorter transfer time of gases leading to higher radon activities). We propose that in-air ^{222}Rn activities
387 - thanks to the radioactive properties of radon which make it sensitive to degassing kinetics and, hence,
388 degassing depth - could be an interesting monitoring parameter in addition to SO_2 and other
389 geochemical and geophysical methods.

390 *5.4 Radiological effects and radon hazard assessment*

391 **[24]** The European regulations for public exposure to radon (EURATOM, 2013) recommend that radon
392 activity in working places always remains below the threshold of 300 Bq/m^3 because of the potential
393 damages of this radioactive gas to the respiratory system. Exposure to high levels of radon has been
394 recognized as a major cause of lung cancer (Lubin et al., 1995). Two hotspots where radon activities
395 exceed by far this threshold were found on the crater rim of Mt. Etna, on each side of the small hill
396 between the Voragine and Bocca Nuova craters (Fig. 4b). Radon activities as high as 1 kBq/m^3 are rare
397 for outdoor environments and indicate that volcanic exhalations are a major source of radioactivity
398 into the local air. Accordingly, the radon uptake through inhalation may be of concern for those people
399 who either visit the volcano or work on it (e.g., volcano guides, scientists). Radon activities measured
400 at one meter of elevation above the ground are the most relevant to assess the respiratory uptake.
401 For activities between 1.1 and 8.8 kBq/m^3 (Table 1), the radiological dose rate can be calculated in the

range 16-131 µSv/h using a conversion coefficient of $1{,}5.10^{-5}$ mSv per Bq.h.m^{-3} (obtained from a dose coefficient of 6,7 mSv per mJ.h.m^{-3} and an equilibrium factor of 0.4 between radon and its daughters) as recommended by the International Commission on Radiological Protection (norm 137, Paquet et al., 2017). For tourists spending a few tens of minutes at the summit of Mt. Etna once in a lifetime, the equivalent dose transmitted to their body remains very low and most likely harmless. For instance, a tourist walking on the path around the Central Crater, spending 10 minutes close to the Voragine hotspot and 20 minutes on the southern slope, would receive a dose of ca. 27 µSv, which is only 2% of the worldwide typical yearly exposure to radon. However, for volcano guides spending up to 4 hours per day at the summit of the volcano, this on a daily basis all the touristic season long, the dose rate may be significantly higher. In a probable scenario of 30 minutes exposure at the identified radon hotspots once a day, the received radiological dose can be computed as: (131×10'/60' + 16×20'/60') × 10^{-3} (mSv/working day) × 100 (working day/y) (assuming the season peak lasts from early May to late September with 5 working days a week) = 2.7 mSv/yr. This value is twice higher than the typical exposure due to radon (1.26 mSv/yr, UNSCEAR, 2008). Although many other factors - out of the scope of the present study - should be considered in order to refine this assessment (radon daughters concentrations, radioactive aerosol particle size distribution, exact duration of exposure, use of individual protective devices such as gas masks), the present study strongly suggests that radon should be included in future studies on volcanic-gas-related health hazards.

6) Conclusions

[25] This first experiment of radon dosimetry in air at an active volcano revealed free-air radon levels significantly higher than the atmospheric background in the zones most exposed to volcanic gases (up to a few kBq/m^3). Radon in such a dynamic environment could come from diffuse soil degassing, low- to mid-temperature steaming fumaroles and from the main gas plume made of primary magmatic vapor. In the lack of a detailed knowledge of local meteorological effects inside the Central Crater of Mt. Etna, the contribution of each potential source of radon could not be deciphered. However, in the SE sector of the Central Crater, the most exposed to the volcanic plume because of the main regional NW wind, a significant radon enrichment was measured in air at 1 m above the ground. This observation strongly supports high radon concentrations in the main gas plume (≈ 550 Bq/m^3). This is the first direct evidence of primary magmatic gases being significantly enriched in radon, which implies that radon does not completely decay away within magmatic gas bubbles before reaching the surface. The transfer time of gases between the degassing reservoir and the surface is thus as short as a few days, or a few weeks at most, thus supporting previous theoretical studies.

[26] The main degassing pathways, either through open vents or through fracture systems, are markedly identified by radon hotspots with free-air activities above 1,000 Bq/m^3 and up to 8,800 Bq/m^3. This observation confirms that radon is a useful geochemical tracer of shallow degassing processes at active volcanoes. Furthermore, an increase of radon free-air activity in the SE sector, most exposed to the crater plume, was observed during an episode of eruptive activity, starting in July 2018 and characterized by increasing SO_2 fluxes, volcanic tremor and surface manifestations. Interestingly,

442 radon activities increased up to 15 times during the volcanic unrest. Such pattern is best explained by
443 a 15-day shorter transfer time of gases from a constant volume of magma, or in other words by
444 degassing occurring at shallower depth beneath the active craters. The results of the study should
445 encourage further studies on radon in volcanic plumes in order to fully appraise the potential of radon
446 monitoring in ambient air at active volcanoes as a useful tool for volcano monitoring, in complement
447 to other geochemical and geophysical parameters. While passive dosimetry appears of interest as an
448 easy-to-deploy and cheap technology to characterize the baseline of in-air radon activities, efficient
449 volcanic monitoring will require more sophisticated technologies with near-real time response (e.g.,
450 Terray et al., 2020). In particular, it will be of the utmost importance to quantify radon fluxes of primary
451 magmatic origin and to understand how they may vary in relation with shallow magma dynamics.

452 **[27]** Finally, radon activities higher than 1 kBq/m^3 found at some places of Mt. Etna summit area could
453 cause health concern for regular workers on the volcano. Further studies should be devoted to a
454 detailed radiological study of exposure to radon of volcanic origin in order to propose individual actions
455 leading to a mitigation of potential health effects.

456

457

458 **Contributions and Acknowledgments**

459 **[28]** LT, VB and PJG designed the passive dosimetry experiment and set it in the field with the help of
460 OS and others (Clarisse Mallet, LMGE Clermont-Ferrand, Jean-Luc Devidal, LMV Clermont-Ferrand and
461 Romain Lauzeral, McGill University Montréal) who are warmly thanked. F. Muré is acknowledged for

462 his technical assistance in the management of FLAME SO_2 flux measurement network. All authors
463 contributed to the ideas presented in this paper and to its writing. We thank the Associate Editor and
464 anonymous reviewers for their meaningful suggestions and comments which led to improve the
465 manuscript.

466 **[29]** The scientific support of INGV - Osservatorio Etneo and the logistical help provided by both Parco
467 dell'Etna, Funivia dell'Etna and Gruppo Guide Alpine Etna Sud & Nord were essential for the success
468 of this study. This research is part of the project RAVE@Etna that has received funding from the
469 European Union's Horizon 2020 research and innovation program under grant agreement N° 654182.
470 This is Laboratory of Excellence ClerVolc contribution number XXX [NB: ClerVolc number will be
471 communicated once the manuscript is accepted for publication].

472 **[30]** In order to comply with FAIR standards, the two datasets presented in the manuscript (radon
473 measurements presented in Table 1 and daily SO_2 flux data provided in Figure 6) are archived in zenodo
474 general repository (https://zenodo.org/) with the DOI 10.5281/zenodo.3560896. These datasets can
475 be found at https://zenodo.org/record/3560896.

476

477 **References**

478 Aiuppa, A., Giudice, G., Gurrieri, S., Liuzzo, M., Burton, M., Caltabiano, T., McGonigle,
479 A.J.S., Salerno, G., Shinohara, H., Valenza, M., 2008. Total volatile flux from Mount
480 Etna. Geophysical Research Letters 35. https://doi.org/10.1029/2008GL035871
481 Allard, P., Aiuppa, A., Bani, P., Métrich, N., Bertagnini, A., Gauthier, P.-J., Shinohara, H.,
482 Sawyer, G., Parello, F., Bagnato, E., Pelletier, B., Garaebiti, E., 2016. Prodigious
483 emission rates and magma degassing budget of major, trace and radioactive volatile
484 species from Ambrym basaltic volcano, Vanuatu island Arc. Journal of Volcanology

and Geothermal Research, Understanding volcanoes in the Vanuatu arc 322, 119–143. https://doi.org/10.1016/j.jvolgeores.2015.10.004
Andres, R., Rose, W., Stoiber, R., Williams, S., Matías, O., Morales, R., 1993. A summary of sulfur dioxide emission rate measuremnts from Guatemalan volcanoes. Bull Volcanol 55, 379–388. https://doi.org/10.1007/BF00301150
Berlo, K., Turner, S., Blundy, J., Black, S., Hawkesworth, C., 2006. Tracing pre-eruptive magma degassing using (210Pb/226Ra) disequilibria in the volcanic deposits of the 1980–1986 eruption of Mount St. Helens. Earth and Planetary Science Letters 249, 337–349. https://doi.org/10.1016/j.epsl.2006.07.018
Bollettino settimanale sul monitoraggio vulcanico, geochimico e sismico del vulcano Etna, 20/08/2018 - 26/08/2018, 2018. INGV-OE.
Bonaccorso, A., Calvari, S., Coltelli, M., Del Negro, C., Falsaperla, S., 2004. Mt. Etna: Volcano Laboratory. Washington DC American Geophysical Union Geophysical Monograph Series 143. https://doi.org/10.1029/GM143
Campion, R., Salerno, G.G., Coheur, P.-F., Hurtmans, D., Clarisse, L., Kazahaya, K., Burton, M., Caltabiano, T., Clerbaux, C., Bernard, A., 2010. Measuring volcanic degassing of SO2 in the lower troposphere with ASTER band ratios. Journal of Volcanology and Geothermal Research 194, 42–54. https://doi.org/10.1016/j.jvolgeores.2010.04.010
Chirkov, A.M., 1975. Radon as a possible criterion for predicting eruptions as observed at Karymsky volcano. Bull Volcanol 39, 126–131. https://doi.org/10.1007/BF02596952
Cigolini, C., Laiolo, M., Coppola, D., Trovato, C., Borgogno, G., 2016. Radon surveys and monitoring at active volcanoes: learning from Vesuvius, Stromboli, La Soufrière and Villarrica. Geological Society, London, Special Publications 451, 183–208. https://doi.org/10.1144/SP451.1
Condomines, M., Sigmarsson, O., Gauthier, P.J., 2010. A simple model of 222Rn accumulation leading to 210Pb excesses in volcanic rocks. Earth and Planetary Science Letters 293, 331–338. https://doi.org/10.1016/j.epsl.2010.02.048
Corsaro, R.A., Andronico, D., Behncke, B., Branca, S., Caltabiano, T., Ciancitto, F., Cristaldi, A., De Beni, E., La Spina, A., Lodato, L., Miraglia, L., Neri, M., Salerno, G., Scollo, S., Spata, G., 2017. Monitoring the December 2015 summit eruptions of Mt. Etna (Italy): Implications on eruptive dynamics. Journal of Volcanology and Geothermal Research 341, 53–69. https://doi.org/10.1016/j.jvolgeores.2017.04.018
De Beni, E., Cantarero, M., Messina, A., 2019. UAVs for volcano monitoring: A new approach applied on an active lava flow on Mt. Etna (Italy), during the 27 February–02 March 2017 eruption. Journal of Volcanology and Geothermal Research 369, 250–262. https://doi.org/10.1016/j.jvolgeores.2018.12.001
De Novellis, V., Atzori, S., Luca, C.D., Manzo, M., Valerio, E., Bonano, M., Cardaci, C., Castaldo, R., Bucci, D.D., Manunta, M., Onorato, G., Pepe, S., Solaro, G., Tizzani, P., Zinno, I., Neri, M., Lanari, R., Casu, F., 2019. DInSAR Analysis and Analytical Modeling of Mount Etna Displacements: The December 2018 Volcano-Tectonic Crisis. Geophysical Research Letters 46, 5817–5827. https://doi.org/10.1029/2019GL082467
Delmelle, P., Stix, J., Baxter, P., Garcia-Alvarez, J., Barquero, J., 2002. Atmospheric dispersion, environmental effects and potential health hazard associated with the low-altitude gas plume of Masaya volcano, Nicaragua. Bull Volcanol 64, 423–434. https://doi.org/10.1007/s00445-002-0221-6
EURATOM, 2013. Directive laying down basic safety standards for protection against the dangers arising from exposure to ionising radiation [WWW Document]. URL https://eur-lex.europa.eu/eli/dir/2013/59/oj (accessed 10.9.19).

Gauthier, P.-J., Condomines, M., 1999. 210Pb–226Ra radioactive disequilibria in recent lavas and radon degassing: inferences on the magma chamber dynamics at Stromboli and Merapi volcanoes. Earth and Planetary Science Letters 172, 111–126. https://doi.org/10.1016/S0012-821X(99)00195-8

Gauthier, P.-J., Condomines, M., Hammouda, T., 1999. An experimental investigation of radon diffusion in an anhydrous andesitic melt at atmospheric pressure: implications for radon degassing from erupting magmas. Geochimica et Cosmochimica Acta 63, 645–656. https://doi.org/10.1016/S0016-7037(98)00305-6

Gauthier, P.-J., Le Cloarec, M.-F., Condomines, M., 2000. Degassing processes at Stromboli volcano inferred from short-lived disequilibria (210Pb–210Bi–210Po) in volcanic gases. Journal of Volcanology and Geothermal Research 102, 1–19. https://doi.org/10.1016/S0377-0273(00)00179-7

Gauthier, P.-J., Sigmarsson, O., Gouhier, M., Haddadi, B., Moune, S., 2016. Elevated gas flux and trace metal degassing from the 2014–2015 fissure eruption at the Bárðarbunga volcanic system, Iceland. Journal of Geophysical Research: Solid Earth 121, 1610–1630. https://doi.org/10.1002/2015JB012111

Giammanco, S., Melián, G., Neri, M., Hernández, P.A., Sortino, F., Barrancos, J., López, M., Pecoraino, G., Perez, N.M., 2016. Active tectonic features and structural dynamics of the summit area of Mt. Etna (Italy) revealed by soil CO2 and soil temperature surveying. Journal of Volcanology and Geothermal Research 311, 79–98. https://doi.org/10.1016/j.jvolgeores.2016.01.004

Giammanco, S., Sims, K.W.W., Neri, M., 2007. Measurements of 220Rn and 222Rn and CO2 emissions in soil and fumarole gases on Mt. Etna volcano (Italy): Implications for gas transport and shallow ground fracture. Geochemistry, Geophysics, Geosystems 8. https://doi.org/10.1029/2007GC001644

Gill, J., Williams, R., Bruland, K., 1985. Eruption of basalt and andesite lava degasses 222Rn and 210Po. Geophysical Research Letters 12, 17–20. https://doi.org/10.1029/GL012i001p00017

Hansell, A., Oppenheimer, C., 2004. Health Hazards from Volcanic Gases: A Systematic Literature Review. Archives of Environmental Health: An International Journal 59, 628–639. https://doi.org/10.1080/00039890409602947

Jacobi, W., André, K., 1963. The vertical distribution of radon 222, radon 220 and their decay products in the atmosphere. Journal of Geophysical Research (1896-1977) 3799–3814. https://doi.org/10.1029/JZ068i013p03799@10.1002/(ISSN)2156-2202.TGNARA1

Lambert, G., Bristeau, P., Polian, G., 1976. Emission and enrichments of radon daughters from Etna Volcano magma. Geophysical Research Letters 3, 724–726. https://doi.org/10.1029/GL003i012p00724

Lambert, G., Le Cloarec, M.F., Ardouin, B., Le Roulley, J.C., 1985. Volcanic emission of radionuclides and magma dynamics. Earth and Planetary Science Letters 76, 185–192. https://doi.org/10.1016/0012-821X(85)90158-X

Le Cloarec, M.-F., Gauthier, P.-J., 2003. Merapi Volcano, Central Java, Indonesia: A case study of radionuclide behavior in volcanic gases and its implications for magma dynamics at andesitic volcanoes: RADIONUCLIDE BEHAVIOR IN VOLCANIC GASES. Journal of Geophysical Research: Solid Earth 108. https://doi.org/10.1029/2001JB001709

Le Cloarec, M.F., Pennisi, M., 2001. Radionuclides and sulfur content in Mount Etna plume in 1983–1995: new constraints on the magma feeding system. Journal of Volcanology and Geothermal Research 108, 141–155. https://doi.org/10.1016/S0377-0273(00)00282-1

583 Liotta, M., Paonita, A., Caracausi, A., Martelli, M., Rizzo, A., Favara, R., 2010.
584 Hydrothermal processes governing the geochemistry of the crater fumaroles at Mount
585 Etna volcano (Italy). Chemical Geology 278, 92–104.
586 https://doi.org/10.1016/j.chemgeo.2010.09.004
587 Lubin, J.H., Boice, J.D., Edling, C., Hornung, R.W., Howe, G.R., Kunz, E., Kusiak, R.A.,
588 Morrison, H.I., Radford, E.P., Samet, J.M., Tirmarche, M., Woodward, A., Yao, S.X.,
589 Pierce, D.A., 1995. Lung Cancer in Radon-Exposed Miners and Estimation of Risk
590 From Indoor Exposure. J Natl Cancer Inst 87, 817–827.
591 https://doi.org/10.1093/jnci/87.11.817
592 Marchese, F., Genzano, N., Neri, M., Falconieri, A., Mazzeo, G., Pergola, N., 2019. A Multi-
593 Channel Algorithm for Mapping Volcanic Thermal Anomalies by Means of Sentinel-2
594 MSI and Landsat-8 OLI Data. Remote Sensing 11, 2876.
595 https://doi.org/10.3390/rs11232876
596 Marchese, F., Neri, M., Falconieri, A., Lacava, T., Mazzeo, G., Pergola, N., Tramutoli, V.,
597 2018. The Contribution of Multi-Sensor Infrared Satellite Observations to Monitor Mt.
598 Etna (Italy) Activity during May to August 2016. Remote Sensing 10, 1948.
599 https://doi.org/10.3390/rs10121948
600 Mollo, S., Tuccimei, P., Soligo, M., Galli, G., Scarlato, P., 2018. Chapter 18 - Advancements
601 in Understanding the Radon Signal in Volcanic Areas: A Laboratory Approach Based
602 on Rock Physicochemical Changes, in: Samui, P., Kim, D., Ghosh, C. (Eds.),
603 Integrating Disaster Science and Management. Elsevier, pp. 309–328.
604 https://doi.org/10.1016/B978-0-12-812056-9.00018-X
605 Monnin, M.M., 2001. Radon Over Volcanic and Seismic Areas, in: Frontasyeva, M.V.,
606 Perelygin, V.P., Vater, P. (Eds.), Radionuclides and Heavy Metals in Environment,
607 NATO Science Series. Springer Netherlands, Dordrecht, pp. 319–330.
608 https://doi.org/10.1007/978-94-010-0993-5_44
609 Morales-Simfors, N., Wyss, R.A., Bundschuh, J., 2020. Recent progress in radon-based
610 monitoring as seismic and volcanic precursor: A critical review. Critical Reviews in
611 Environmental Science and Technology 50, 979–1012.
612 https://doi.org/10.1080/10643389.2019.1642833
613 Neri, M., Ferrera, E., Giammanco, S., Currenti, G., Cirrincione, R., Patanè, G., Zanon, V.,
614 2016. Soil radon measurements as a potential tracer of tectonic and volcanic activity.
615 Scientific Reports 6, 24581. https://doi.org/10.1038/srep24581
616 Neri, M., Maio, M.D., Crepaldi, S., Suozzi, E., Lavy, M., Marchionatti, F., Calvari, S.,
617 Buongiorno, M.F., 2017. Topographic Maps of Mount Etna's Summit Craters,
618 updated to December 2015. Journal of Maps 13, 674–683.
619 https://doi.org/10.1080/17445647.2017.1352041
620 Paquet, F., Bailey, M.R., Leggett, R.W., Lipsztein, J., Marsh, J., Fell, T.P., Smith, T., Nosske,
621 D., Eckerman, K.F., Berkovski, V., 2017. ICRP Publication 137: Occupational Intakes
622 of Radionuclides: Part 3. Annals of the ICRP 46, 1–486.
623 Salerno, G.G., Burton, M., Di Grazia, G., Caltabiano, T., Oppenheimer, C., 2018. Coupling
624 Between Magmatic Degassing and Volcanic Tremor in Basaltic Volcanism. Front.
625 Earth Sci. 6. https://doi.org/10.3389/feart.2018.00157
626 Salerno, G.G., Burton, M.R., Oppenheimer, C., Caltabiano, T., Randazzo, D., Bruno, N.,
627 Longo, V., 2009a. Three-years of SO2 flux measurements of Mt. Etna using an
628 automated UV scanner array: Comparison with conventional traverses and
629 uncertainties in flux retrieval. Journal of Volcanology and Geothermal Research 183,
630 76–83. https://doi.org/10.1016/j.jvolgeores.2009.02.013
631 Salerno, G.G., Burton, M.R., Oppenheimer, C., Caltabiano, T., Tsanev, V.I., Bruno, N.,
632 2009b. Novel retrieval of volcanic SO2 abundance from ultraviolet spectra. Journal of

Volcanology and Geothermal Research 181, 141–153. https://doi.org/10.1016/j.jvolgeores.2009.01.009
Sato, K., Kaneoka, I., Sato, J., 1980. Rare-gas releasing experiments and Rn degassing from erupting magma. Geochemical Journal 14, 91–94. https://doi.org/10.2343/geochemj.14.91
Scollo, S., Prestifilippo, M., Pecora, E., Corradini, S., Merucci, L., Spata, G., Coltelli, M., 2014. Eruption column height estimation of the 2011-2013 Etna lava fountains. Annals of Geophysics 57, 0214. https://doi.org/10.4401/ag-6396
Seidel, J.L., Monnin, M., 1984. Mesures de Radon-222 dans le sol de l'Etna (Sicile): 1980–1983. Bull Volcanol 47, 1071–1077. https://doi.org/10.1007/BF01952363
Sigmarsson, O., Condomines, M., Gauthier, P.-J., 2015. Excess 210Po in 2010 Eyjafjallajökull tephra (Iceland): Evidence for pre-eruptive gas accumulation. Earth and Planetary Science Letters 427, 66–73. https://doi.org/10.1016/j.epsl.2015.06.054
Sources and effects of ionizing radiation, UNSCEAR 2008 Report, 2010. . Volume I. Annex A. United Nations, New York.
Terray, L., Gauthier, P.-J., Salerno, G., Caltabiano, T., La Spina, A., Sellitto, P., Briole, P., 2018. A New Degassing Model to Infer Magma Dynamics from Radioactive Disequilibria in Volcanic Plumes. Geosciences 8, 27. https://doi.org/10.3390/geosciences8010027
Terray, L., Royer, L., Sarramia, D., Achard, C., Bourdeau, E., Chardon, P., Claude, A., Fuchet, J., Gauthier, P.-J., Grimbichler, D., Mezhoud, J., Ogereau, F., Vandaële, R., Breton, V., 2020. From Sensor to Cloud: An IoT Network of Radon Outdoor Probes to Monitor Active Volcanoes. Sensors 20, 2755. https://doi.org/10.3390/s20102755
Tokonami, S., Iimoto, T., Kurosawa, R., 1996. Continuous measurement of the equilibrium factor F and the unattached fraction fp of radon progeny in the environment. Environment International, The Natural Radiation Environment VI 22, 611–616. https://doi.org/10.1016/S0160-4120(96)00163-8
Vaupotič, J., Žvab, P., Giammanco, S., 2010. Radon in outdoor air in the Mt. Etna area, Italy. Nukleonika Vol. 55, No. 4, 573–577.
Wu, Z., Huang, N.E., Long, S.R., Peng, C.-K., 2007. On the trend, detrending, and variability of nonlinear and nonstationary time series. Proceedings of the National Academy of Sciences 104, 14889–14894.
Zimmer, M., Erzinger, J., 2003. Continuous H2O, CO2, 222Rn and temperature measurements on Merapi Volcano, Indonesia. Journal of Volcanology and Geothermal Research, Understanding volcanoes through multiparameter measurements and their interpretation: In memory of Bruno Martinelli 125, 25–38. https://doi.org/10.1016/S0377-0273(03)00087-8

675

676

677

678

679

680

681

682

683 **Figures and tables**

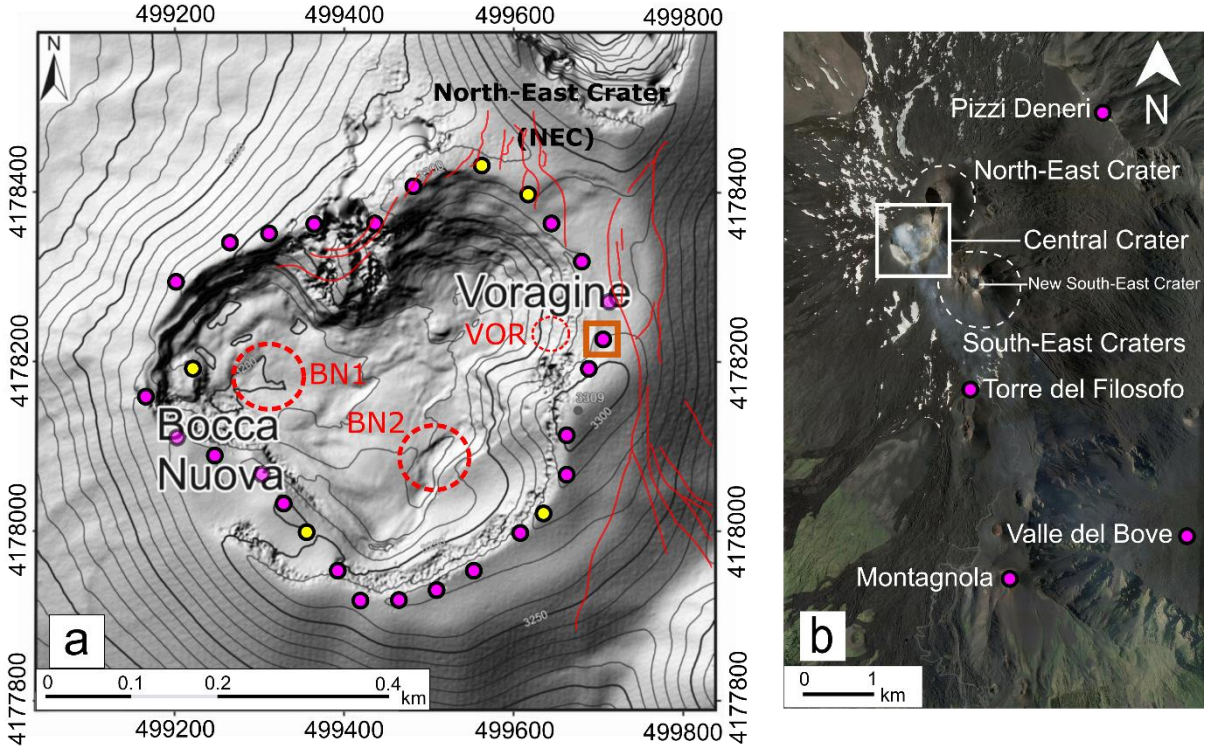

Figure 1: *(a) Map of the summit craters of Mt. Etna (modified from Neri et al., 2017) with the location of the radon dosimetry stations (yellow dots represent the stations that were replaced in July and purple dots the other stations). Dotted red circles represent the degassing vents active during the period of exposure of dosimeters. VOR stands for the Voragine vent and BN1-BN2 for the two Bocca Nuova vents. The radon hotspot in front of VOR vent (see text for details) is indicated with an orange frame. Red lines depict the main North-South fractures formed on the rim after the May 2016 eruption (drawn after Marchese et al., 2018) (b) Wider view of Mt. Etna summit area (extracted from Google Earth) with the position of the four remote reference dosimetry stations. The white frame corresponds to the map in (a).*

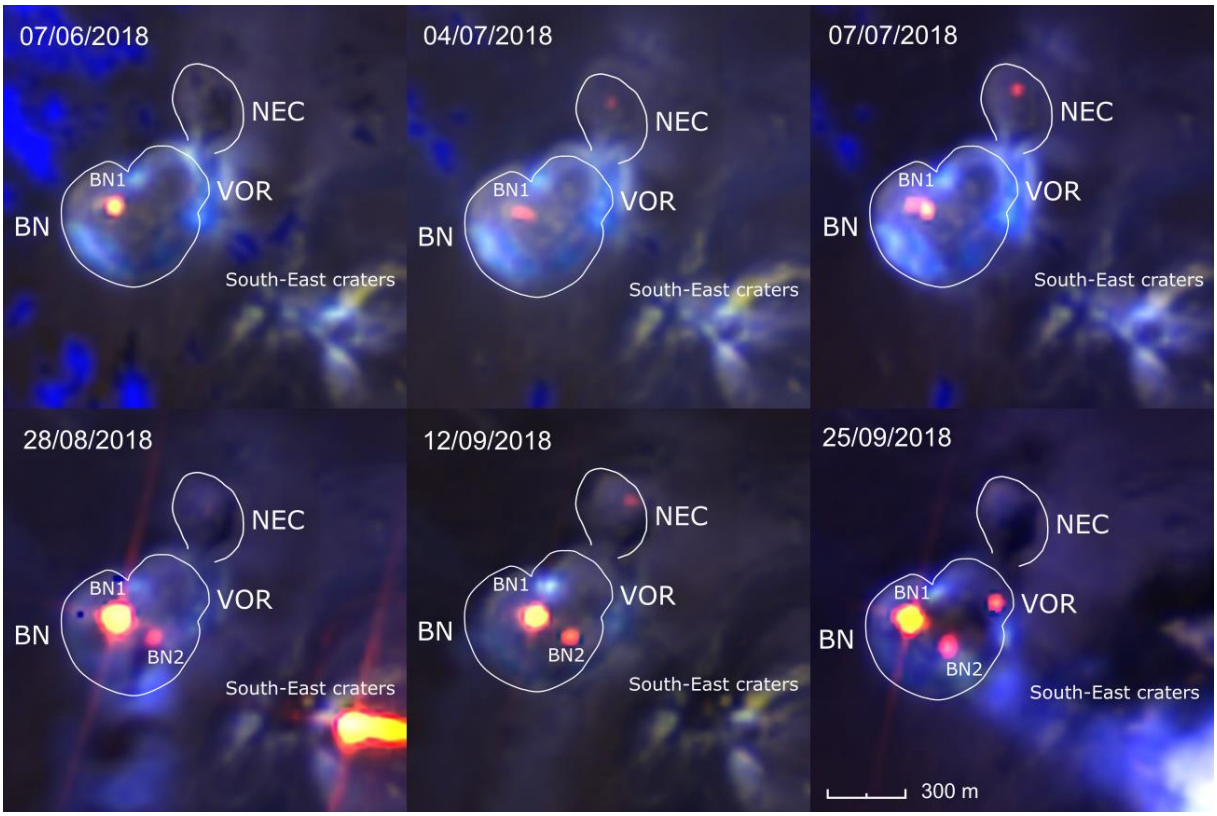

Figure 2: *Mt. Etna summit craters seen from Sentinel 2B satellite during summer 2018. Images on the top correspond with the first exposure period (24/05/18-06/07/18, the last image has been captured one day after on 07/07/2018) and images on the bottom correspond to the second period (06/07/18-11/10/18). Images have been produced using a combination of bands from the L2A level (orthorectified bottom-of-atmosphere reflectance) as follows: Red (Band 12 – Short Wave Infra Red – 2190 nm) – Green (Band 11 – Short Wave Infra Red – 1610 nm) – Blue (Band 9 – Water vapour – 945 nm). The spatial resolution is 20m for bands 12 and 11 but 60m for band 9. Sentinel products are made publicly available by the European Spatial Agency on its website (https://apps.sentinel-hub.com/eo-browser/). Red and yellow pixels highlight positive infrared thermal anomalies that correspond to the precise location of degassing vents BN1 (Bocca Nuova 1), BN2 (Bocca Nuova 2) and VOR (Voragine), possibly related to the presence of very shallow magma. The gas plume escaping from the crater, as well as the main fumarole fields, are also visible in blue due to their high water content.*

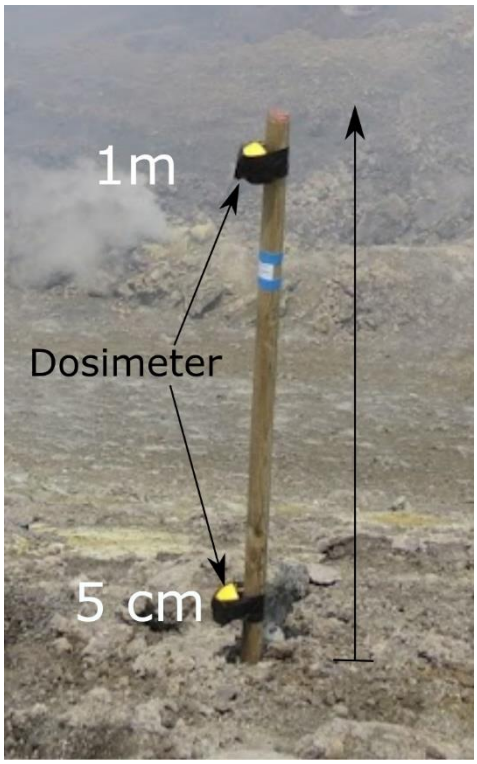

Figure 3: *Image of a station installed on the rim of Etna Central Crater. Two dosimeters are fixed to a wooden stick anchored to the ground: one at 5 cm above the ground and another one at 1 m above the ground.*

Figure 4: *Spatial distribution of ground level (5 cm, left panel) and in free air (1 m, right panel) integrated radon activities measured in the four different sectors of Mt. Etna Central Crater. References stations are represented separately below each panel. All crater stations are positioned according to the geographical coordinates given in Table 1. Coordinates are displayed using an UTM (Universal Transverse Mercator) projection relatively to the center of the Central Crater (barycenter of all station locations). Black star symbols correspond to stations where radon activities could be determined, black cross symbols correspond to stations where no radon activity is available (see text for explanations) and the red star symbol correspond to the Voragine hotspot station (see text). Radon activity values are indicated next to each station pictogram and for the few stations replaced in July 2018 the time-weighted mean value over the two exposure periods is given . A colored band is also drawn to reflect the spatial distribution of activity values. The color sequence all around the crater is obtained from a linear interpolation of measured activity in angular coordinates. Voragine station outlier values are excluded from the color band and the colorscale is logarithmic. The wind rose obtained from Trapani radiosounding (see text for details) is also represented with a polar histogram. Circles correspond to iso-lines of percentage of occurrence for wind directions. The bin color refer to the wind speed (see legend on the right side).*

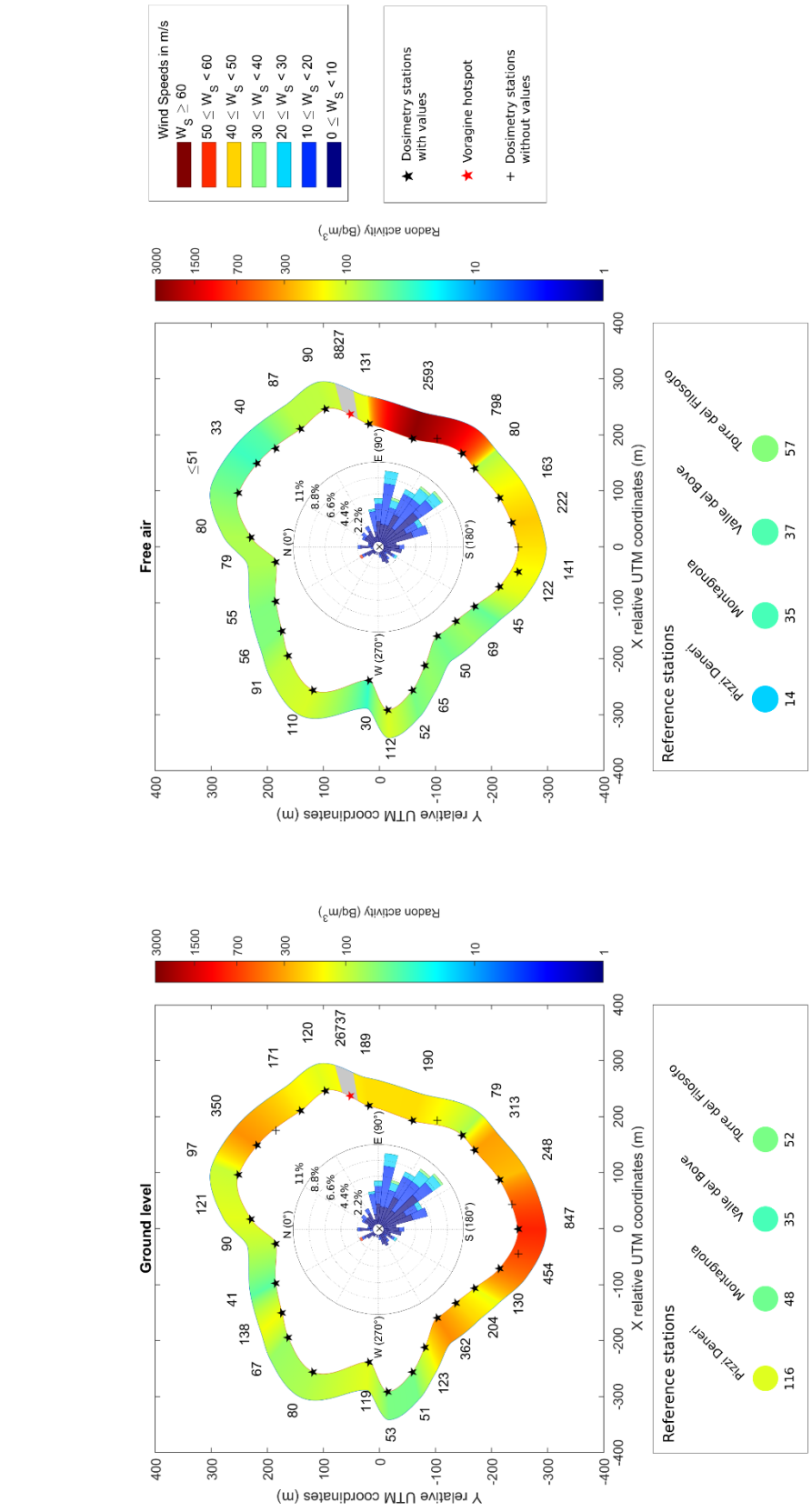
Free air
Ground level
Wind Speeds in m/s
$W_S \geq 60$
$50 \leq W_S < 60$
$40 \leq W_S < 50$
$30 \leq W_S < 40$
$20 \leq W_S < 30$
$10 \leq W_S < 20$
$0 \leq W_S < 10$
Dosimetry stations with values
Voragine hotspot
Dosimetry stations without values
Radon activity (Bq/m³)
3000
1500
700
300
100
10
1
Y relative UTM coordinates (m)
X relative UTM coordinates (m)
N (0°)
E (90°)
S (180°)
W (270°)
11%
8.8%
6.6%
4.4%
2.2%
Reference stations
Pizzi Deneri
Montagnola
Valle del Bove
Torre del Filosofo
116
48
35
52
14
35
37
57

766

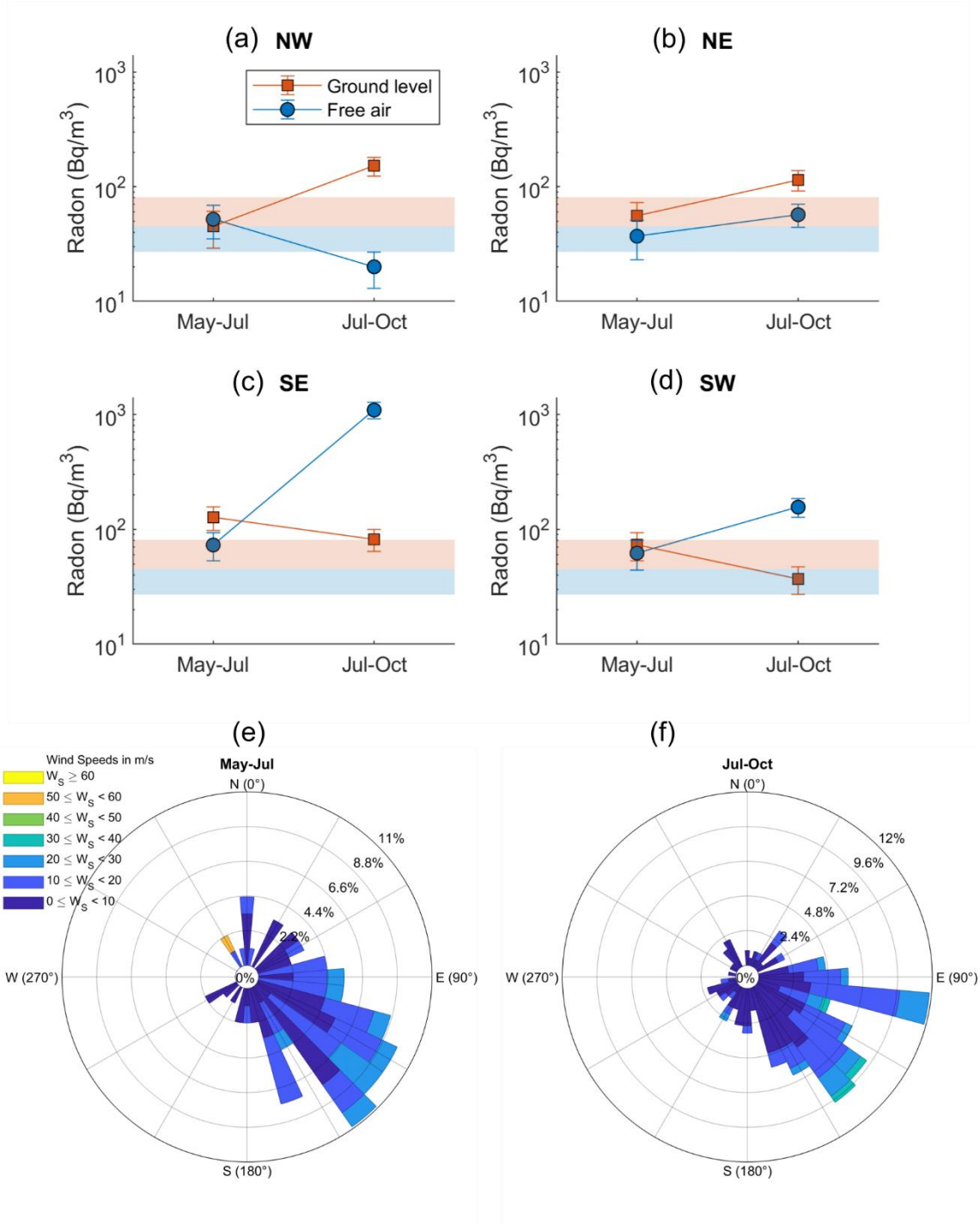

767

768 ***Figure 5:*** *Comparison of ^{222}Rn activity (Fig. 5a to 5d) and wind (Fig. 5e and 5f) between May-July 2018 and July-October*
769 *2018 periods. (a) to (d) - Comparison of ^{222}Rn integrated activity between the two periods for each of the four stations that*
770 *were replaced in July 2018 (one for each sector of the crater rim). Ground level activities correspond to orange square*
771 *symbols, whereas free-air activities are depicted in blue dot points. Ground-level and free-air reference activities measured*
772 *at remote locations (mean values are given in Table 1) are also indicated in the plot background with orange and blue*
773 *colors, respectively. The same wooden stick was used for the two measurement periods at all stations, except on the NE*
774 *sector where the new station was positioned a few meters away from the former emplacement because of a potential risk of*
775 *destruction due to combustion of the wood. (e) and (f) - Comparison of wind direction and speed between May-July 2018*
776 *and July-October 2018. For both periods the mean speed was 10 m/s with a standard deviation of 7 m/s.*

777

Table 1 *(next page): Radon dosimeter results with uncertainty for each dosimeter given at confidence interval of 2-σ. For the mean values, uncertainty corresponds to the standard error (standard deviation of the population divided by the square root of the number of elements in the population). Exposure periods started and ended as follows: May-Oct (24/05/18-11/10/18), May-Jul (24/05/18-06/07/18) and Jul-Oct (06/07/18-11/10/18). "lost" indicates a dosimeter that was lost during the experiment, "udl" refers to a dosimeter that yielded results under the detection limit, and "damaged" corresponds to a dosimeter that was corroded by acids and could not be analyzed or that was clogged in soldered dust preventing radon from entering the capsule. Note that one station (namely, that closest to the Voragine vent) was excluded from the computation of the mean value of the NE sector (see text for explanation).*

Station	Lat	Lon	Exposition period	Integrated radon activity (Bq/m^3) Ground level (5cm)	2σ	Free air (1m)	2σ
			References sites				
Pizzi Deneri	37.7636	15.0193	May-Oct	116	22	14	5
Montagnola	37.7177	15.0066	May-Oct	48	10	35	8
Valle del Bove	37.7206	15.0334	Jul-Oct	35	10	37	10
Torre del Filosofo	37.7368	15.0006	May-Oct	52	11	57	12
Reference mean				**63**	**18**	**36**	**9**
			North West sector				
North West sector	37.7508	14.9905	May-Oct	53	12	112	21
North West sector	37.7511	14.9911	May-Jul	45	16	52	17
			Jul-Oct	152	29	20	7
North West sector	37.7520	14.9909	May-Oct	80	16	110	21
North West sector	37.7524	14.9916	May-Oct	67	14	91	18
North West sector	37.7525	14.9921	May-Oct	138	25	56	12
North West sector	37.7526	14.9927	May-Oct	41	10	55	12
NW sector mean				**82**	**17**	**71**	**13**
			North East sector				
North East sector	37.7526	14.9935	May-Oct	90	18	79	16
North East sector	37.7530	14.9940	May-Oct	121	23	80	16
North East sector	37.7532	14.9949	May-Jul	56	17	37	14
			Jul-Oct	115	23	57	13
North East sector	37.7529	14.9955	May-Jul	52	17	*udl*	
			Jul-Oct	480	82	34	10
North East sector	37.7526	14.9958	May-Jul	*lost*		81	20
North East sector	37.7522	14.9962	May-Oct	171	31	87	17
North East sector	37.7518	14.9966	May-Oct	120	22	90	17
North East sector	37.7511	14.9963	May-Oct	189	36	131	27
NE sector mean				**155**	**43**	**75**	**10**
Voragine vent hotspot	37.7514	14.9965	May-Oct	26737	4327	8827	1430
			South East sector				
South East sector	37.7504	14.9960	May-Oct	190	34	2593	422
South East sector	37.7501	11.9960	May-Oct	*damaged*		*damaged*	
South East sector	37.7496	14.9957	May-Jul	127	29	73	20
			Jul-Oct	82	18	1091	180
South East sector	37.7494	14.9954	May-Oct	313	53	80	16
South East sector	37.7490	14.9948	May-Oct	248	43	163	29
South East sector	37.7488	14.9943	May-Oct	*lost*		222	39
South East sector	37.7487	14.9938	May-Oct	847	140	*lost*	
SE sector mean				**301**	**114**	**704**	**409**
			South West sector				
South West sector	37.7487	14.9933	May-Oct	*damaged*		141	26
South West sector	37.7490	14.9930	May-Oct	454	76	122	23
South West sector	37.7494	14.9926	May-Jul	73	20	62	18
			Jul-Oct	37	10	156	29
South West sector	37.7497	14.9923	May-Oct	204	36	69	14
South West sector	37.7500	14.9920	May-Oct	362	51	50	11
South West sector	37.7502	14.9914	May-Oct	123	23	65	13
South West sector	37.7504	14.9909	May-Oct	51	11	52	11
SW sector mean				**186**	**62**	**90**	**15**

Figure 1.

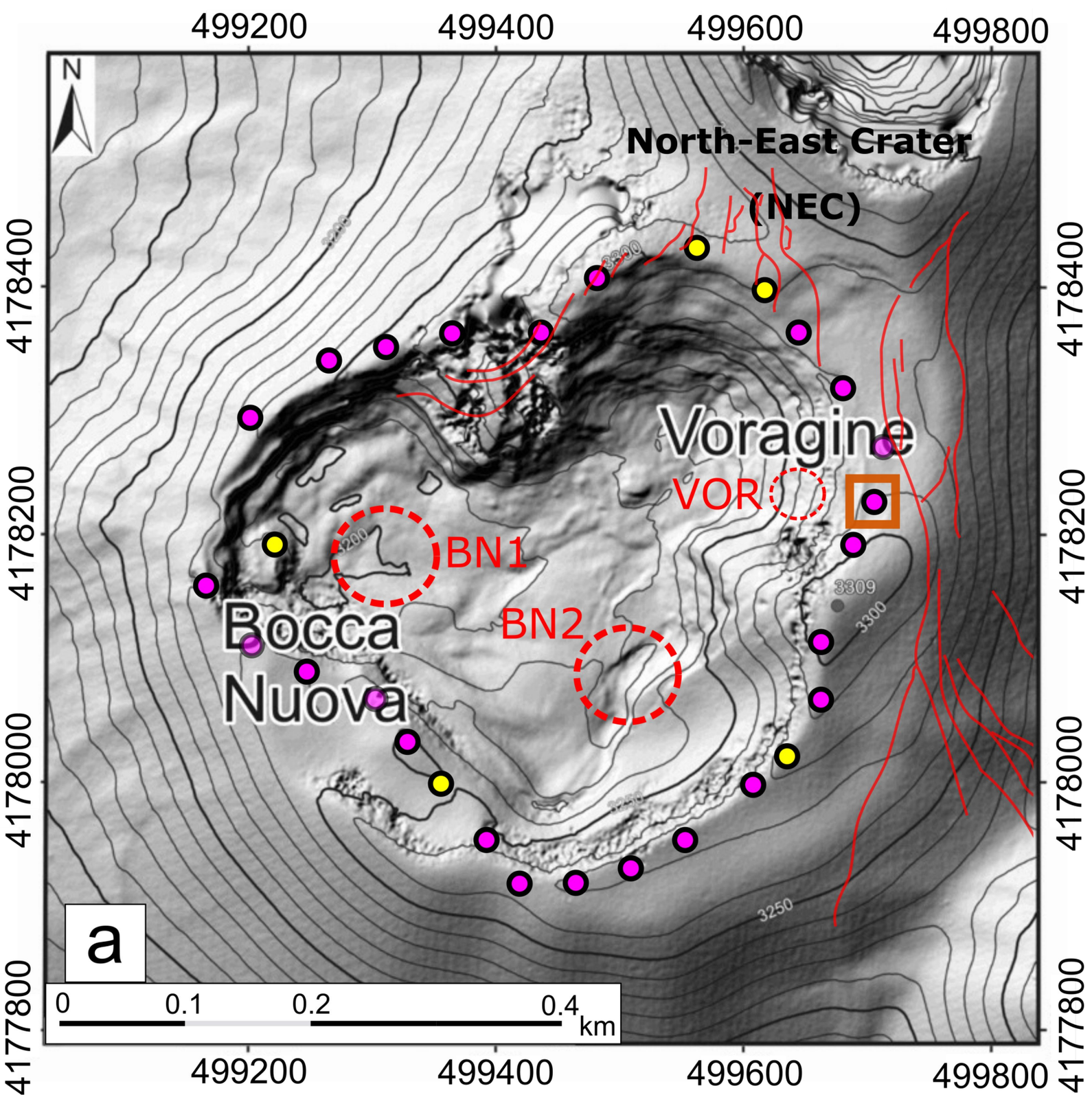
499200
499400
499600
499800
4178400
4178200
4178000
4177800
N
North-East Crater
(NEC)
Voragine
VOR
BN1
BN2
Bocca
Nuova
3309
3300
3250
a
0
0.1
0.2
0.4
km


Pizzi Deneri
N
North-East Crater
Central Crater
New South-East Crater
South-East Craters
Torre del Filosofo
Valle del Bove
Montagnola
b
0
1
km

Figure 2.

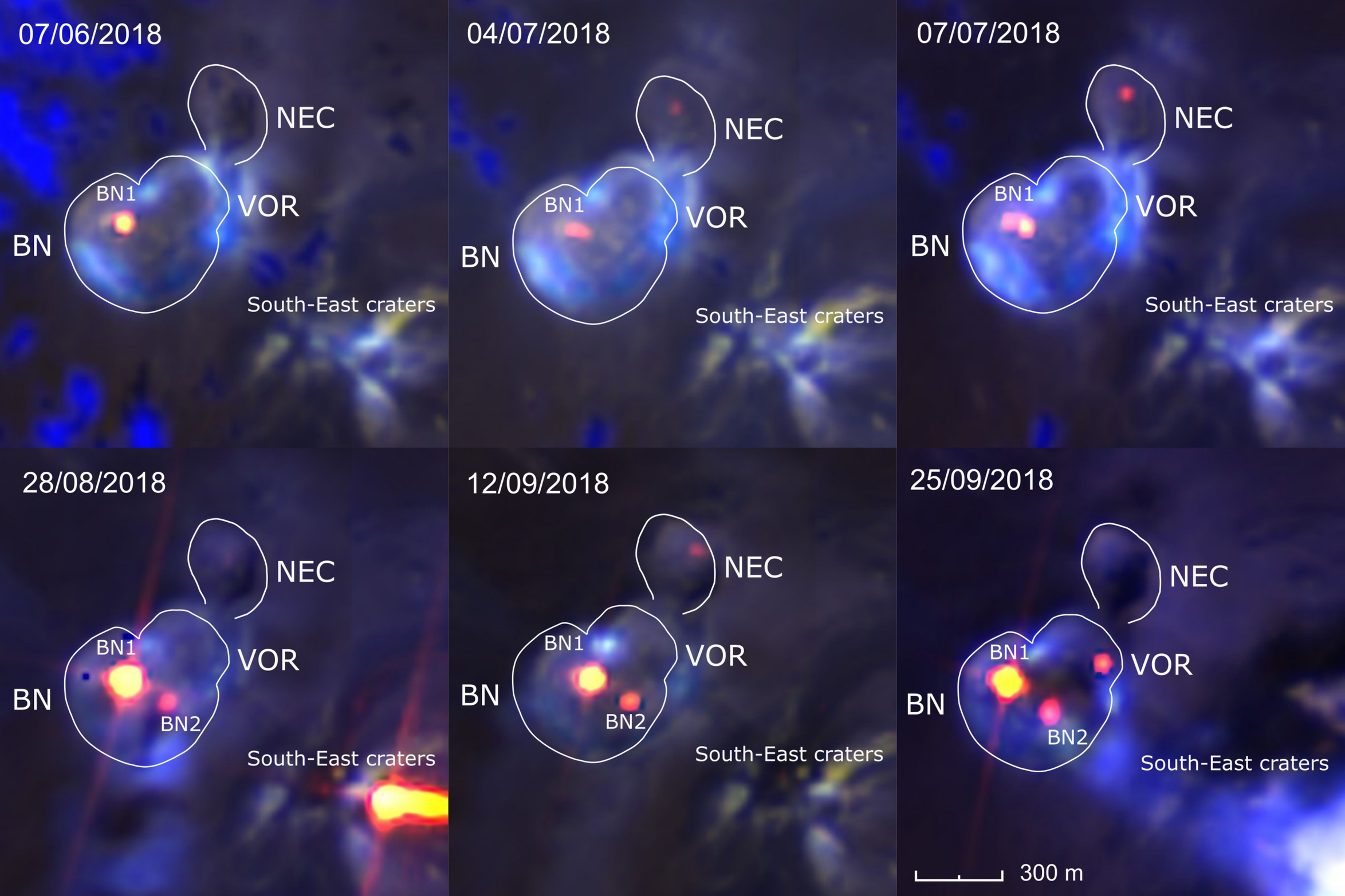
07/06/2018
NEC
BN1
VOR
BN
South-East craters
04/07/2018
NEC
BN1
VOR
BN
South-East craters
07/07/2018
NEC
BN1
VOR
BN
South-East craters
28/08/2018
NEC
BN1
VOR
BN
BN2
South-East craters
12/09/2018
NEC
BN1
VOR
BN
BN2
South-East craters
25/09/2018
NEC
BN1
VOR
BN
BN2
South-East craters
300 m

Figure 3.

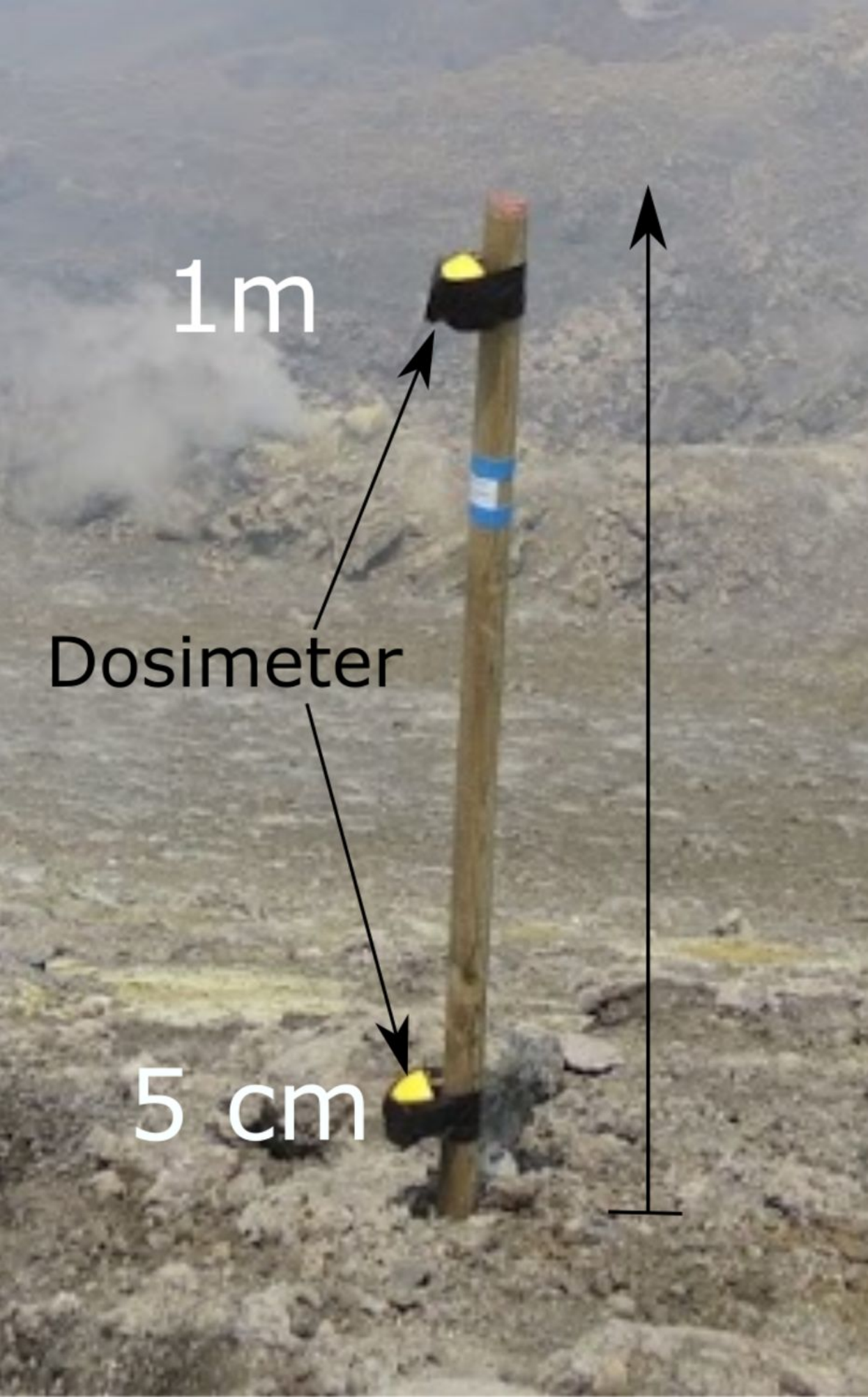
1m
Dosimeter
5 cm

Figure 4.

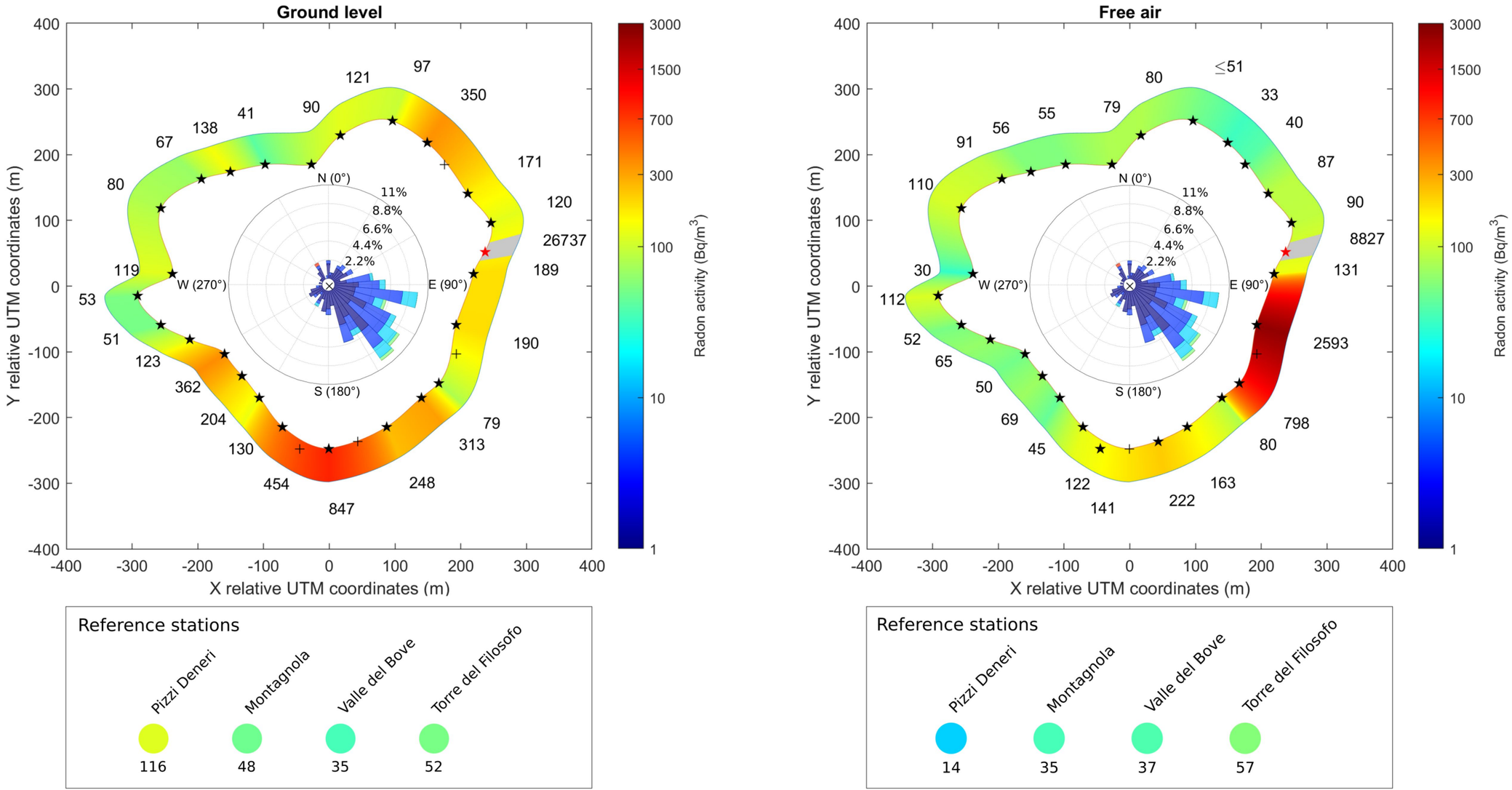
Ground level
Free air
Y relative UTM coordinates (m)
X relative UTM coordinates (m)
Radon activity (Bq/m3)
N (0°)
E (90°)
S (180°)
W (270°)
11%
8.8%
6.6%
4.4%
2.2%
Wind Speeds in m/s
Ws ≥ 60
50 ≤ Ws < 60
40 ≤ Ws < 50
30 ≤ Ws < 40
20 ≤ Ws < 30
10 ≤ Ws < 20
0 ≤ Ws < 10
Dosimetry stations with values
Voragine hotspot
Dosimetry stations without values
Reference stations
Pizzi Deneri
Montagnola
Valle del Bove
Torre del Filosofo
116
48
35
52
14
35
37
57

Figure 5.

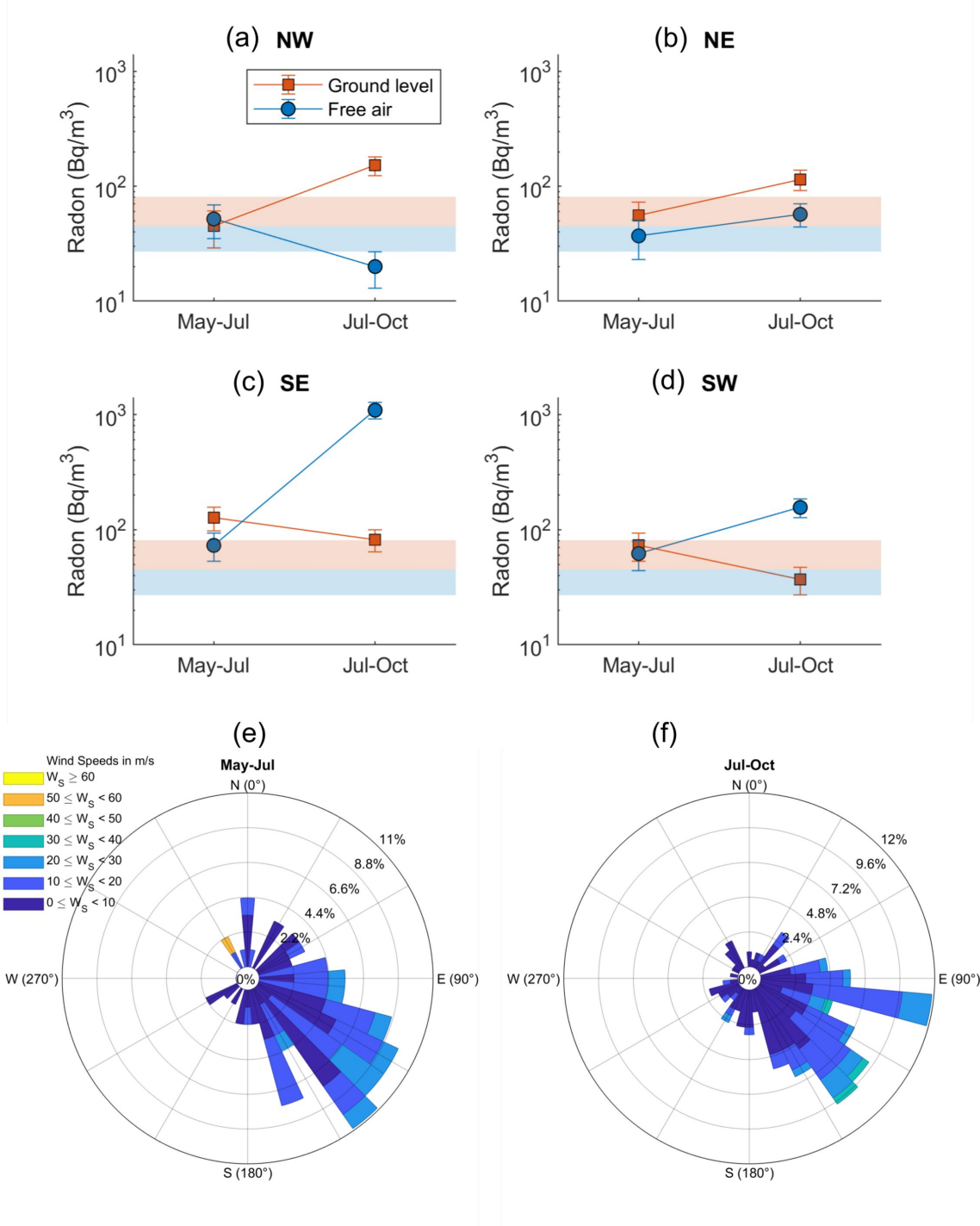
(a) NW
(b) NE
(c) SE
(d) SW
Ground level
Free air
Radon (Bq/m3)
May-Jul
Jul-Oct
(e)
(f)
Wind Speeds in m/s
May-Jul
Jul-Oct
N (0°)
E (90°)
S (180°)
W (270°)